




Generalized matching condition for unity efficiency quantum transduction

Chiao-Hsuan Wang ^{1,2,3,4,*} Mengzhen Zhang ⁴ and Liang Jiang ⁴

¹Department of Physics and Center for Theoretical Physics, National Taiwan University, Taipei 10617, Taiwan

²Center for Quantum Science and Engineering, National Taiwan University, Taipei 10617, Taiwan

³Physics Division, National Center for Theoretical Sciences, Taipei 10617, Taiwan

⁴Pritzker School of Molecular Engineering, University of Chicago, Chicago, Illinois 60637, USA



(Received 5 April 2022; accepted 16 September 2022; published 7 November 2022)

Coherently converting quantum states between distinct elements via quantum transducers remains a crucial yet challenging task in quantum science. Especially in demand is quantum transduction between optical frequencies, which are ideal for low-loss transmission across long distances, and microwave frequencies, which admit high-fidelity quantum operations. We present a generic formalism for N -stage quantum transduction that covers various leading microwave-to-optical, microwave-to-microwave, and optical-to-optical linear conversion approaches. We then identify effective circuit models and the resulting generalized matching conditions for achieving maximum conversion efficiency. The generalized matching condition requires resistance matching as well as frequency matching beyond the usual resonant assumption, with a simple impedance-matched transmission interpretation. Our formalism provides a generic toolbox for determining experimental parameters to realize efficient quantum transduction and suggests different regimes of nonresonant conversions that might outperform all-resonant ones.

DOI: [10.1103/PhysRevResearch.4.L042023](https://doi.org/10.1103/PhysRevResearch.4.L042023)

Global quantum networks for secured communication, distributed quantum computation, and beyond is among the appealing applications of future quantum technologies [1–4]. Lying at the heart of networking quantum devices are quantum transducers, coherent interfaces that can faithfully transmit quantum information between components with distinct energies [5–7]. Major interests have been placed on coherent conversions between optical and microwave frequencies, with the former ideal for reliable long-range communications through optical fibers or in free space [8,9], and the latter admitting high-fidelity local quantum operations using superconducting processors [10,11].

A variety of physical implementations for direct state transfer between microwave and optical systems have been rapidly developed in the past decade. Direct conversion between microwave and optical frequencies can be established through electro-optics [12–16], electro-optomechanics [17,18], optomagnonics [19,20], piezo-optomechanics [21,22], and atom-assisted conversion schemes that involve two or more intermediate atomic levels [23–27]. Despite the wide range of experimental settings, these approaches can be modeled as multistage coupled bosonic chains with two end modes coupled externally. The same model applies to optomechanical photon-phonon translators [28], microwave-to-microwave

frequency converters [29] in superconducting circuits, and optical-to-optical frequency converters via cavity optomechanics [30] or coupled-resonator optical waveguides through eight-ring resonators [31].

When the environmental thermal noise is negligible or can be fully suppressed by cooling [32,33], the performance of a direct quantum transducer is measured by the transmissivity η , i.e., the coherent conversion efficiency between the input signal and the output signal [34]. A perfect direct quantum transducer should be of unity efficiency and hence can faithfully transfer quantum signals with zero information loss. With more complicated experimental implementations, such as three- to six-wave mixing atom-based transducers [23–25], being pursued, a systematic approach to designing physical parameters for achieving unity efficiency transduction is pressing.

In this Letter, we derive a unity-efficiency-achieving condition inspired by the widely known impedance-matching condition in electrical engineering. Based on this discovery, we establish an effective electric circuit model to clarify the analogy between direct quantum transduction and electrical power transmission. The generality of our unity-efficiency-achieving condition allows us to loosen the stringent constraints imposed on previous quantum transduction schemes, such as the requirement that all involved modes must be on resonance in the rotating frame to achieve maximum efficiency (after consideration of frequency shifts given by the rotating-wave approximation) [17,28,35], which may extend the applicability and flexibility of direct quantum transduction. We also investigate the robustness of this condition and its working range under the influence of environmental dissipation introduced to the intermediate stages.

*chiaowang@phys.ntu.edu.tw

Published by the American Physical Society under the terms of the [Creative Commons Attribution 4.0 International](https://creativecommons.org/licenses/by/4.0/) license. Further distribution of this work must maintain attribution to the author(s) and the published article's title, journal citation, and DOI.

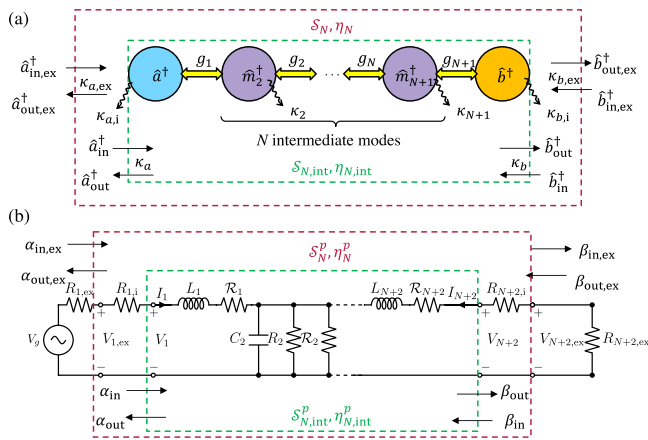


FIG. 1. (a) Schematic of the N -stage quantum transduction system with photon number conversion efficiency η_N and internal photon number conversion efficiency $\eta_{N,\text{int}}$. (b) Schematic of an effective circuit network for N -stage transduction (with odd N) with power efficiency $\eta_N^p = \eta_N$ and internal power efficiency $\eta_{N,\text{int}}^p = \eta_{N,\text{int}}$.

Model of N -stage direct quantum transduction. The transduction device we are considering is a bosonic chain consisting of $N + 2$ modes, where each mode in this chain is coupled to their nearest neighbors through passive interactions [Fig. 1(a)] regardless of their physical carriers (e.g. optical modes, microwave modes, acoustic modes, magnons, etc.). The implementation of such systems has been demonstrated in existing quantum transduction experiments [12–31] by properly driving the involved modes. The whole device can be described by the following Hamiltonian,

$$\hat{H}_N = - \sum_{j=1}^{N+2} \Delta_j \hat{m}_j^\dagger \hat{m}_j + \sum_{j=1}^{N+1} g_j (\hat{m}_j^\dagger \hat{m}_{j+1} + \hat{m}_{j+1}^\dagger \hat{m}_j), \quad (1)$$

with $\hat{m}_j, \hat{m}_j^\dagger$ the annihilation and creation operators of each mode, Δ_j the detuning of each mode in the rotating frame, and g_j the coupling strength of each interaction. To stress the presence of the intermediate modes, we address each of them as a *stage*. Therefore, a device with $N + 2$ modes contains N stages as the intermediate modes. For similar reasons, we use \hat{a} as an alternative denotation for \hat{m}_1 and \hat{b} for \hat{m}_{N+2} as shown in Fig. 1(a).

For transduction, this device will be passively coupled with external channels to receive the input signal $\hat{a}_{\text{in,ex}}^\dagger$ at the rate $\kappa_{a,\text{ex}}$ and to emit the output signal $\hat{b}_{\text{out,ex}}^\dagger$ at the rate $\kappa_{b,\text{ex}}$, requiring the modes \hat{a}^\dagger and \hat{b}^\dagger to be of disparate frequencies (e.g., \hat{a}^\dagger may be a microwave mode while \hat{b}^\dagger is an optical mode). Taking environmental dissipation into consideration, we introduce an intrinsic loss rate κ_j for each mode. The intrinsic loss rates for the first and the last modes are referred to as $\kappa_{a,i}$ and $\kappa_{b,i}$, respectively, to be consistent with our conventions. Thus, the rates $\kappa_a = \kappa_{a,i} + \kappa_{a,\text{ex}}$ and $\kappa_b = \kappa_{b,i} + \kappa_{b,\text{ex}}$ are used to denote the total dissipation rates of the two modes. Similarly, the other parameters $\Delta_1, \Delta_{N+2}, g_1, g_{N+1}$ are referred to as $\Delta_a, \Delta_b, g_a, g_b$, respectively.

The conversion efficiency η of the transducer quantifies the fraction of photon (boson) number power that can be

successfully transferred from one end to the other. Treating the N -stage transducer as a scattering matrix \mathcal{S}_N between the external input and output modes as shown by the red dashed boundary in Fig. 1(a), the photon number conversion efficiency from \hat{a}^\dagger to \hat{b}^\dagger is defined as $\eta_N \equiv |\mathcal{S}_N \hat{b}_{\text{out,ex}}^\dagger \hat{a}_{\text{in,ex}}^\dagger|^2$. Here, we have been focused on the scheme of a bosonic chain with only nearest-neighbor beam-splitter interactions such that there is neither nonreciprocity [36] nor amplification effects [37]. A perfect transduction is well defined in this scenario by the unity efficiency condition $\eta_N = 1$.

The N -stage conversion efficiency at a signal frequency ω can be expressed in a general form [38]

$$\eta_N[\omega] = \frac{\kappa_{a,\text{ex}} \kappa_{b,\text{ex}}}{\kappa_a \kappa_b} \left| \frac{\sqrt{\kappa_a \kappa_b} \prod_{j=1}^{N+1} i g_j}{\prod_{j=1}^{N+2} \chi_{j,\text{eff}}^{-1}} \right|^2 = \eta_{\text{ext}} \eta_{N,\text{int}}[\omega], \quad (2)$$

where $\chi_{j,\text{eff}}$ is the effective susceptibility for \hat{m}_j^\dagger , a modification to the bare mode susceptibility $\chi_j \equiv [i(\omega + \Delta_j) + \kappa_j/2]^{-1}$, due to the couplings $g_j, \dots, g_{N+1} (= g_b)$,

$$\chi_{j,\text{eff}}^{-1} \equiv \chi_j^{-1} + \frac{g_j^2}{\chi_{j+1}^{-1} + \frac{g_{j+1}^2}{\chi_{j+2}^{-1} + \frac{g_{j+2}^2}{\chi_{j+3}^{-1} + \frac{g_{j+3}^2}{\chi_{j+4}^{-1} + \frac{g_{j+4}^2}{\chi_{j+5}^{-1} + \frac{g_{j+5}^2}{\chi_b^{-1}}}}}}. \quad (3)$$

Here, $\eta_{\text{ext}} = \kappa_{a,\text{ex}} \kappa_{b,\text{ex}} / \kappa_a \kappa_b$ is the external conversion efficiency and $\eta_{N,\text{int}}[\omega]$ is the N -stage internal conversion efficiency.

The internal efficiency $\eta_{N,\text{int}}[\omega]$ can be understood as the efficiency of the internal scattering process $\mathcal{S}_{N,\text{int}}$ as shown by the green dashed boundary in Fig. 1(a). The relevant scattering modes are the total input and output modes $\hat{a}^\dagger (\hat{b}^\dagger)_{\text{in/out}}$ coupled to $\hat{a}^\dagger (\hat{b}^\dagger)$ at an overall rate $\kappa_{a(b)}$, due to the interaction with both the external channels and the dissipative environment.

The external efficiency η_{ext} , on the other hand, represents the average fraction of information that can be successfully transferred through the external channels, without being lost to the dissipative environments at rates $\kappa_{a,i}$ and $\kappa_{b,i}$, while leaving or entering the end modes \hat{a}^\dagger and \hat{b}^\dagger . In the strong external coupling limit such that $\kappa_{a,\text{ex}} \gg \kappa_{a,i}$ and $\kappa_{b,\text{ex}} \gg \kappa_{b,i}$, one can reach maximal external efficiency $\eta_{\text{ext}} = 1$. We will thus focus on the general criteria for system parameters to attain unity internal conversion efficiency. Since the system dynamics is invariant under a global energy shift, we will use $\nu_j \equiv \omega + \Delta_j$ as the relevant frequency variables.

As a starting example, we study the simplest case of 0-stage transduction [Fig. 2(b)] relevant for electro-optical quantum transducers [12–16]. The 0-stage internal efficiency is

$$\eta_{0,\text{int}} = \left| \frac{g \sqrt{\kappa_b \kappa_a}}{g^2 + \chi_a^{-1} \chi_b^{-1}} \right|^2. \quad (4)$$

Under the traditional all-resonant assumption $\nu_a (\equiv \omega + \Delta_a) = \nu_b (\equiv \omega + \Delta_b) = 0$, the matching condition to fulfill $\eta_{1,\text{int}} = 1$ was given by $C_{a,b} \equiv 4g^2 / \kappa_a \kappa_b = 1$, where $C_{a,b}$ is the cooperativity between modes \hat{a}^\dagger and \hat{b}^\dagger [28]. On the other hand, two off-resonant peaks in efficiency have also been observed in the strong-coupling regime $C_{a,b} > 1$ with

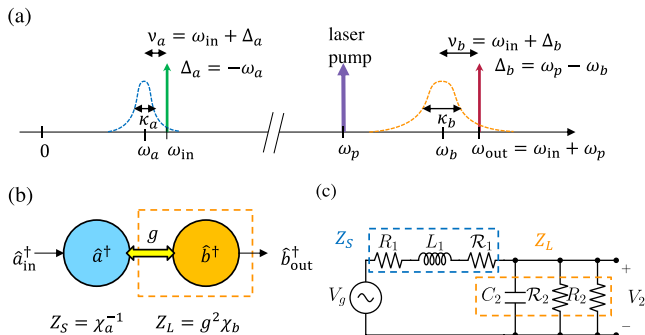


FIG. 2. (a) An exemplar frequency diagram for 0-stage transduction from \hat{a}^\dagger to \hat{b}^\dagger in the laboratory frame. Here, $\omega_{a(b)}$ is the frequency of mode \hat{a}^\dagger (\hat{b}^\dagger) and $\omega_{in(out)}$ is the frequency of the input (output) signal. The system can be described with a time-independent Hamiltonian as in Eq. (1) by moving \hat{b}^\dagger and $\hat{b}_{out,ex}^\dagger$ to the rotating frame at the laser pump frequency ω_p that mediates the linear up- and down-conversion. (b) Schematic of the 0-stage quantum transduction model. (c) Effective circuit model that reproduces the 0-stage internal conversion efficiency by setting $L_1 = 1$, $\mathcal{R}_1 = i\Delta_a$, $R_1 = \kappa_a/2$, $C_2 = 1/g^2$, $\mathcal{R}_2 = g^2/(i\Delta_b)$, and $R_2 = 2g^2/\kappa_b$.

$\kappa_a = \kappa_b$ [39]. However, there is no systematic analysis of these off-resonant peaks.

A natural question arises: What is the most general condition to achieve unity internal conversion efficiency? Solving for the solution of $v_a \equiv \omega + \Delta_a$ given $\eta_{0,int}[\omega] = 1$, we arrive at a set of independent criteria

$$v_a = \frac{g^2 v_b}{v_b^2 + \kappa_b^2/4}, \quad (5)$$

$$\kappa_a = \frac{g^2 \kappa_b}{v_b^2 + \kappa_b^2/4}, \quad (6)$$

where $v_b \equiv \omega + \Delta_b$. The all-resonant condition $v_a = v_b = 0$ fulfills the nonlinear condition of Eq. (5), which might have other solutions. Before proceeding with the general solution to the matching condition, we would like to point out that the conditions of Eqs. (5) and (6) admit an impedance-matching interpretation analogous to the electric circuit power transfer theory.

Impedance-matching interpretation for unity efficiency transduction. In electric circuits, for an active voltage transferred from a source impedance Z_S to a load impedance Z_L , maximum transfer power is obtained if the conjugate impedance-matching condition $Z_L = Z_S^*$ is satisfied [40]. For the 0-stage transduction system, unity internal conversion efficiency is also achieved when the system has impedance-matched parameters. Viewed from the \hat{a}^\dagger port, $\chi_{a,eff}^{-1}$ is modified by $g^2 \chi_b$ due to the coupling with the \hat{b}^\dagger mode. By interpreting the original inverse susceptibility of mode \hat{a}^\dagger as the source impedance in the unit of rates, $Z_S = \chi_a^{-1}$, and the coupling-induced inverse susceptibility modification as the load impedance, $Z_L = g^2 \chi_b$, the first condition Eq. (5) is equivalent to having $\text{Im}[\chi_a^{-1}] = -\text{Im}[g^2 \chi_b]$ while the second condition Eq. (6) corresponds to $\text{Re}[\chi_a^{-1}] = \text{Re}[g^2 \chi_b]$, which altogether fulfill $Z_L = Z_S^*$.

To construct a rigorous connection between maximal conversion efficiency for transducers and the impedance-matching condition for electric circuits, we now establish an effective circuit model. Specifically, the effective circuit shown in Fig. 1(b) can reproduce an identical frequency response as an N -stage quantum transducer in Fig. 1(a) with an odd N , such that the electric power internal efficiency is the same as the photon number internal efficiency $\eta_{N,int}^p[\omega] = \eta_{N,int}[\omega]$, by setting [38]

$$\begin{aligned} L_j^{-1} C_{j+1}^{-1} &= g_j^2, & R_j L_j^{-1} &= \kappa_j/2, & \mathcal{R}_j L_j^{-1} &= i\Delta_j, & \text{odd } j, \\ C_j^{-1} L_{j+1}^{-1} &= g_j^2, & G_j C_j^{-1} &= \kappa_j/2, & \mathcal{G}_j C_j^{-1} &= i\Delta_j, & \text{even } j. \end{aligned} \quad (7)$$

The circuit is composed of elements with inductance $L_j \in \mathbb{R}$, capacitance $C_j \in \mathbb{R}$, resistance $R_j = 1/G_j \in \mathbb{R}$, and generalized resistance $\mathcal{R}_j = 1/\mathcal{G}_j \in i\mathbb{R}$. The resistance at the two ends can be separated into external coupling and intrinsic loss components, $R_{1(N+2),ex} L_{1(N+2)}^{-1} = \kappa_{a(b),ex}/2$ and $R_{1(N+2),i} L_{1(N+2)}^{-1} = \kappa_{a(b),i}/2$, to replicate the total conversion efficiency $\eta_N^p[\omega] = \eta_N[\omega]$. Here, we have introduced the *generalized* resistance of imaginary values \mathcal{R}_j to account for the independent mode detunings Δ_j , which is distinct from prior numerical [41] or synthetic methods [42,43] for coupled resonator arrays.

With the explicit circuit correspondence, we see a clear analogy between the scattering process of the input/output modes, \hat{a}^\dagger (\hat{b}^\dagger)_{in/out}, for transducers and the incident/reflective power waves, α (β)_{in/out}, for electric circuits [40,44,45]. With the effective circuit parameters shown in Fig. 2(c), the impedance-matching analogy for attaining unity 0-stage internal efficiency naturally follows through.

Generalized matching condition. We now extend the concept of impedance matching to N -stage quantum transduction. An impedance-matching condition viewed from the \hat{a}^\dagger mode (taking $L_1 = 1$) reads

$$(\chi_a^{-1})^* = g_a^2 \chi_{2,eff}. \quad (8)$$

When all the intermediate modes are lossless, $\kappa_2 = \dots = \kappa_{N+1} = 0$, this condition also leads to impedance matching viewed from the \hat{b}^\dagger mode (taking L_{N+2} or $C_{N+2} = 1$),

$$(\chi_b^{-1})^* = g_b^2 \chi_{N+1,eff,r}, \quad (9)$$

where $\chi_{j,eff,r}$ is the effective susceptibility of mode j viewed from the reversed direction due to the couplings $g_1 (= g_a), \dots, g_{j-1}$,

$$\chi_{j,eff,r}^{-1} \equiv \chi_j^{-1} + \frac{g_{j-1}^2}{\chi_{j-1}^{-1} + \frac{g_a^2}{\chi_a^{-1}}}. \quad (10)$$

One can achieve $\eta_{N,int} = 1$ by requiring a lossless condition $\kappa_2 = \dots = \kappa_{N+1} = 0$ together with an impedance-matching condition Eq. (8) or (9).

There exist additional physical interpretations for the above matching conditions Eqs. (8) and (9). First, they give rise to zero internal reflections. Similar to the fact that the power wave reflection coefficient at the source, $r_S^p = (Z_L -$

$Z_S^*/(Z_L + Z_S)$, vanishes for a conjugate matched lossless electric circuit, the above conditions also suggest zero internal reflection for the transducer. Specifically, the internal reflection coefficients are given by

$$r_{N,a} = \mathcal{S}_{N,\text{int}} \hat{a}_{\text{out}}^\dagger \hat{a}_{\text{in}}^\dagger = \frac{g_a^2 \chi_{2,\text{eff}} - (\chi_a^{-1})^*}{g_a^2 \chi_{2,\text{eff}} + \chi_a^{-1}}, \quad (11)$$

$$r_{N,b} = \mathcal{S}_{N,\text{int}} \hat{b}_{\text{out}}^\dagger \hat{b}_{\text{in}}^\dagger = \frac{g_b^2 \chi_{N+1,\text{eff},r} - (\chi_b^{-1})^*}{g_b^2 \chi_{N+1,\text{eff},r} + \chi_b^{-1}}. \quad (12)$$

It is clear that Eq. (8) implies $r_{N,a} = 0$ while Eq. (9) implies $r_{N,b} = 0$. Second, the matching conditions also correspond to critical effective cooperativities along the transduction chain when the system is lossless,

$$C_{j,j+1}^{\text{eff}} \equiv \frac{g_j^2}{(\chi_{j,\text{eff},r}^{-1})^* \chi_{j+1,\text{eff}}} = 1. \quad (13)$$

We summarize the generalized N -stage matching condition in a matrix determinant form [38],

$$M_N = 0, \quad (14)$$

$$M_N \equiv \begin{vmatrix} -(\chi_a^{-1})^* & ig_a & 0 & \cdots & \cdots & 0 \\ ig_a & \chi_2^{-1} & ig_2 & \ddots & & \vdots \\ 0 & ig_2 & \ddots & \ddots & \ddots & \vdots \\ \vdots & \ddots & \ddots & \ddots & \ddots & 0 \\ \vdots & & \ddots & \ddots & \ddots & ig_b \\ 0 & \cdots & \cdots & 0 & ig_b & \chi_b^{-1} \end{vmatrix} \stackrel{\kappa_2 = \cdots = \kappa_{N+1} = 0}{=} \quad (15)$$

We call the real part of the equation the generalized resistance matching condition, $\text{Re } M_N = 0$ and the imaginary part of the equation the generalized resonant condition, $\text{Im } M_N = 0$.

The generalized matching condition Eq. (14) takes a symmetric form in a and b . For example, the generalized 0-stage matching condition reads

$$M_0 = 0 \Rightarrow \begin{cases} \text{Re} : g^2 = \frac{\kappa_a \kappa_b}{4} + \nu_a \nu_b, \\ \text{Im} : \frac{\nu_a}{\kappa_a} = \frac{\nu_b}{\kappa_b}, \end{cases} \quad (16)$$

$$(17)$$

which is mathematically equivalent to the previous set of criteria Eqs. (5) and (6) for getting $\eta_{0,\text{int}}[\omega] = 1$.

Note that in quantum transduction systems there exist Δ_j degrees of freedom associated with the generalized resistance of imaginary values, which are unavailable in real-world linear electric circuits where the resistors are always real. The above expression is thus a generalized version of a matching condition beyond the all-resonant assumption $\forall j, \nu_j \equiv \omega + \Delta_j = 0$, which corresponds to circuits with purely real resistors while setting the signal frequency to be zero, $\omega = 0$, in the rotating frame.

Tuning the off-resonant frequencies. In a typical analysis, the frequencies ν_j 's, after including the frequency shifts given by the rotating-wave approximation, if any, are often chosen to be zero (all resonant) in order to achieve maximum conversion efficiency [17,28,35]. Here, we consider generic schemes such that ν_j 's may be nonzero (off resonant) to offer extra tunability for transduction. One might adjust the system

TABLE I. Optimal frequencies for 0-stage transduction.

$N = 0$	$C_{a,b} > 1$	$C_{a,b} \leq 1$
$\nu_a \equiv \omega + \Delta_a$	$\pm \frac{\kappa_a}{2} \sqrt{C_{a,b} - 1}$	0
$\nu_b \equiv \omega + \Delta_b$	$\pm \frac{\kappa_b}{2} \sqrt{C_{a,b} - 1}$	0
$\eta_{0,\text{int}}^{\text{max}}$	1	$\frac{4C_{a,b}}{(C_{a,b}+1)^2}$

parameters to achieve an ideal conversion for output signal frequencies detuned from ω_b . In the strong-coupling regime $C_{a,b} > 1$ of 0-stage transduction, unity internal efficiency is achieved with nonresonant frequencies $\nu_a \neq 0$ and $\nu_b \neq 0$. The optimal frequencies and the maximal internal efficiency for a given $C_{a,b}$ are summarized in Table I. Note that the transduction process still follows energy conservation even with nonresonant ν_j 's. For example, $\omega_{\text{out}} = \omega_{\text{in}} + \omega_p$ is always true for the 0-stage case shown in Fig. 2(a), while ν_j 's merely represent the frequency differences between the input/output signals and modes \hat{a}^\dagger or \hat{b}^\dagger .

The extra degrees of freedom given by nonresonant ν_j 's can also serve as optimizable parameters in experiments. In practice, the loss rate of the intermediate modes may be non-negligible, and the system can no longer satisfy $M_N = 0$ to reach unity internal efficiency. The mode cooperativities $C_{j,j+1} \equiv 4g_j^2/(\kappa_j \kappa_{j+1})$ are thus finite and limited by experimental constraints. On the other hand, the frequencies and detunings of the modes are typically tunable by laser drives. In such experimental settings, one can find the optimal ν_j 's that lead to maximal efficiency at the given values of $C_{j,j+1}$'s.

We find that the optimal parameters with intermediate losses can again be interpreted as impedance-matched parameters of lossy circuits. Take the case of 1-stage transduction, appropriate for electro-optomechanical [17,18], optomagnetical [19,20], or piezo-optomechanical [21,22] quantum transducers, for example. When $\kappa_2 \neq 0$, we can define mode cooperativities $C_{a,2} = g_a^2/\kappa_a \kappa_2$ and $C_{2,b} = g_b^2/\kappa_2 \kappa_b$. When one of the modes is overcoupled, for instance, if $C_{a,2} > C_{2,b} + 1$, a relevant regime for piezo-optomechanical transducers in which the microwave mode is over coupled [21,22], the maximal internal efficiency is achieved by the choice of optimal frequencies satisfying $(\chi_a^{-1})^* = g_a^2/(\chi_2^{-1} + g_b^2 \chi_b)$ and $\nu_b = 0$. This corresponds to impedance matching at the \hat{a}^\dagger mode while treating \hat{m}_2^\dagger and \hat{b}^\dagger altogether as the load. If $|C_{a,2} - C_{2,b}| \leq 1$, the conversion is optimized when the system is all resonant. This condition can again be understood as an impedance-matched lossy circuit while treating the middle mode as a lossy component partly in the source and partly in the load [38].

For 0-, 1-, and 2-stage transduction, we identify the regimes where maximal internal conversion efficiency is achieved with off-resonant frequencies $\nu_j \equiv \omega + \Delta_j \neq 0$ in the parameter space of mode cooperativities as shown in Fig. 3 [38]. These examples manifest the exotic behavior that a quantum transducer operating at off-resonant frequencies may outperform all-resonant ones.

Our method may be extended for conversion through an ensemble of intermediate modes. For instance, considering

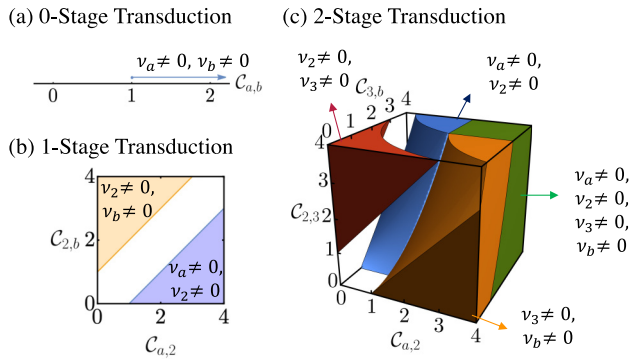


FIG. 3. Phase diagrams for 0-, 1-, and 2-stage transduction in the parameter space of mode cooperativities. In the colored regimes, maximal internal efficiency is achieved with off-resonant frequencies as labeled.

transduction schemes mediated by two excited levels of a large number of atoms N_A [24,25], we can treat the atomic excited states as collective modes $\hat{S}_{2(3)} = \frac{1}{\sqrt{N_A}} \sum_k \hat{m}_{2(3),k}$ and obtain the same form of conversion efficiency as in Eq. (2) but with enhanced coupling rates $g_{a(b)} \rightarrow \sqrt{N_A} g_{a(b)}$. To include the effect of inhomogeneous broadening by taking the continuous limit $\sum_k \rightarrow N \int_{-\infty}^{\infty} d\omega_{2,k} d\omega_{3,k} \rho(\omega_{2,k}) \rho(\omega_{3,k})$ and assuming Lorentzian energy level distributions $\rho(\omega_{2(3),k}) = \frac{\Gamma_{2(3)}/2\pi}{(\omega_{2(3),k} - \omega_{2(3)})^2 + (\Gamma_{2(3)}/2)^2}$, one can show that the updated conversion efficiency formula is associated with the broadened

linewidth $\kappa_{2(3)} \rightarrow \kappa_{2(3)} + \Gamma_{2(3)}$. We may also expand our discussion to include thermal noise, which will introduce added noise to the transduction [38].

Conclusion and outlook. In conclusion, we have presented the generalized matching condition for N -stage quantum transduction and suggested different regimes of nonresonant conversions that can outperform all-resonant ones. Moreover, we drew a rigorous connection between transducer models and electric circuits, which brought the available circuit design toolboxes into this field. While our discussion has been focused on quantum transducers, it may also apply to general physical systems described by the externally coupled bosonic-chain model for other applications including microwave photon detectors [46], optical delay lines [47], and optical buffers [48]. Our work provides a generic formalism for determining experimental parameters to realize efficient quantum transduction in various platforms, with potential future extensions for transduction schemes utilizing two-mode-squeezing interactions [49,50] or inhomogeneous couplings of the mediating ensemble.

We thank V. Ferreira, O. Painter, H. Tang, and C. Zou for helpful discussions. We acknowledge support from the ARO (W911NF-18-1-0020, W911NF-18-1-0212), ARO MURI (W911NF-16-1-0349, W911NF-21-1-0325), AFOSR MURI (FA9550-19-1-0399, FA9550-21-1-0209), AFRL (FA8649-21-P-0781), DoE Q-NEXT, NSF (OMA-1936118, EEC-1941583, OMA-2137642), NTT Research, and the Packard Foundation (2020-71479).

- [1] C. Elliott, Building the quantum network, *New J. Phys.* **4**, 46 (2002).
- [2] H. J. Kimble, The quantum internet, *Nature (London)* **453**, 1023 (2008).
- [3] P. Kómár, E. M. Kessler, M. Bishop, L. Jiang, A. S. Sørensen, J. Ye, and M. D. Lukin, A quantum network of clocks, *Nat. Phys.* **10**, 582 (2014).
- [4] C. Simon, Towards a global quantum network, *Nat. Photonics* **11**, 678 (2017).
- [5] N. Lauk, N. Sinclair, S. Barzanjeh, J. P. Covey, M. Saffman, M. Spiropulu, and C. Simon, Perspectives on quantum transduction, *Quantum Sci. Technol.* **5**, 020501 (2020).
- [6] N. J. Lambert, A. Rueda, F. Sedlmeir, and H. G. L. Schwefel, Coherent conversion between microwave and optical photons—An overview of physical implementations, *Adv. Quantum Technol.* **3**, 1900077 (2020).
- [7] X. Han, W. Fu, C.-L. Zou, L. Jiang, and H. X. Tang, Microwave-optical quantum frequency conversion, *Optica* **8**, 1050 (2021).
- [8] H. Takesue, S. D. Dyer, M. J. Stevens, V. Verma, R. P. Mirin, and S. W. Nam, Quantum teleportation over 100 km of fiber using highly efficient superconducting nanowire single-photon detectors, *Optica* **2**, 832 (2015).
- [9] J. Yin, Y. Cao, Y. H. Li, S. K. Liao, L. Zhang, J. G. Ren, W. Q. Cai, W. Y. Liu, B. Li, H. Dai, G. B. Li, Q. M. Lu, Y. H. Gong, Y. Xu, S. L. Li, F. Z. Li, Y. Y. Yin, Z. Q. Jiang, M. Li, J. J. Jia *et al.*, Satellite-based entanglement distribution over 1200 kilometers, *Science* **356**, 1140 (2017).
- [10] A. Blais, A. L. Grimsmo, S. M. Girvin, and A. Wallraff, Circuit quantum electrodynamics, *Rev. Mod. Phys.* **93**, 025005 (2021).
- [11] A. Joshi, K. Noh, and Y. Y. Gao, Quantum information processing with bosonic qubits in circuit QED, *Quantum Sci. Technol.* **6**, 033001 (2021).
- [12] M. Tsang, Cavity quantum electro-optics, *Phys. Rev. A* **81**, 063837 (2010).
- [13] C. Javerzac-Galy, K. Plekhanov, N. R. Bernier, L. D. Toth, A. K. Feofanov, and T. J. Kippenberg, On-chip microwave-to-optical quantum coherent converter based on a superconducting resonator coupled to an electro-optic microresonator, *Phys. Rev. A* **94**, 053815 (2016).
- [14] A. Rueda, F. Sedlmeir, M. C. Collodo, U. Vogl, B. Stiller, G. Schunk, D. V. Strekalov, C. Marquardt, J. M. Fink, O. Painter, G. Leuchs, and H. G. L. Schwefel, Efficient microwave to optical photon conversion: an electro-optical realization, *Optica* **3**, 597 (2016).
- [15] L. Fan, C. L. Zou, R. Cheng, X. Guo, X. Han, Z. Gong, S. Wang, and H. X. Tang, Superconducting cavity electro-optics: A platform for coherent photon conversion between superconducting and photonic circuits, *Sci. Adv.* **4**, eaar4994 (2018).
- [16] W. Fu, M. Xu, X. Liu, C. L. Zou, C. Zhong, X. Han, M. Shen, Y. Xu, R. Cheng, S. Wang, L. Jiang, and H. X. Tang, Cavity electro-optic circuit for microwave-to-optical conversion in the quantum ground state, *Phys. Rev. A* **103**, 053504 (2021).
- [17] R. W. Andrews, R. W. Peterson, T. P. Purdy, K. Cicak, R. W. Simmonds, C. A. Regal, and K. W. Lehnert, Bidirectional and

- efficient conversion between microwave and optical light, *Nat. Phys.* **10**, 321 (2014).
- [18] A. P. Higginbotham, P. S. Burns, M. D. Urmey, R. W. Peterson, N. S. Kampel, B. M. Brubaker, G. Smith, K. W. Lehnert, and C. A. Regal, Harnessing electro-optic correlations in an efficient mechanical converter, *Nat. Phys.* **14**, 1038 (2018).
- [19] R. Hisatomi, A. Osada, Y. Tabuchi, T. Ishikawa, A. Noguchi, R. Yamazaki, K. Usami, and Y. Nakamura, Bidirectional conversion between microwave and light via ferromagnetic magnons, *Phys. Rev. B* **93**, 174427 (2016).
- [20] N. Zhu, X. Zhang, X. Han, C.-L. Zou, C. Zhong, C.-H. Wang, L. Jiang, and H. X. Tang, Waveguide cavity optomagnonics for microwave-to-optics conversion, *Optica* **7**, 1291 (2020).
- [21] X. Han, W. Fu, C. Zhong, C. L. Zou, Y. Xu, A. A. Sayem, M. Xu, S. Wang, R. Cheng, L. Jiang, and H. X. Tang, Cavity piezo-mechanics for superconducting-nanophotonic quantum interface, *Nat. Commun.* **11**, 3237 (2020).
- [22] M. Mirhosseini, A. Sipahigil, M. Kalaei, and O. Painter, Superconducting qubit to optical photon transduction, *Nature (London)* **588**, 599 (2020).
- [23] J. Han, T. Vogt, C. Gross, D. Jaksch, M. Kiffner, and W. Li, Coherent Microwave-to-Optical Conversion via Six-Wave Mixing in Rydberg Atoms, *Phys. Rev. Lett.* **120**, 093201 (2018).
- [24] J. R. Everts, M. C. Berrington, R. L. Ahlefeldt, and J. J. Longdell, Microwave to optical photon conversion via fully concentrated rare-earth-ion crystals, *Phys. Rev. A* **99**, 063830 (2019).
- [25] J. G. Bartholomew, J. Rochman, T. Xie, J. M. Kindem, A. Ruskuc, I. Craiciu, M. Lei, and A. Faraon, On-chip coherent microwave-to-optical transduction mediated by ytterbium in YVO_4 , *Nat. Commun.* **11**, 3266 (2020).
- [26] H. T. Tu, K. Y. Liao, Z. X. Zhang, X. H. Liu, S. Y. Zheng, S. Z. Yang, X. D. Zhang, H. Yan, and S. L. Zhu, High-efficiency coherent microwave-to-optics conversion via off-resonant scattering, *Nat. Photonics* **16**, 291 (2022).
- [27] F. KimiaeeAsadi, J. W. Ji, and C. Simon, Proposal for transduction between microwave and optical photons using ^{167}Er -doped yttrium orthosilicate, *Phys. Rev. A* **105**, 062608 (2022).
- [28] A. H. Safavi-Naeini and O. Painter, Proposal for an optomechanical traveling wave phonon-photon translator, *New J. Phys.* **13**, 013017 (2011).
- [29] B. Abdo, K. Sliwa, F. Schackert, N. Bergeal, M. Hatridge, L. Frunzio, A. D. Stone, and M. Devoret, Full Coherent Frequency Conversion between Two Propagating Microwave Modes, *Phys. Rev. Lett.* **110**, 173902 (2013).
- [30] J. T. Hill, A. H. Safavi-Naeini, J. Chan, and O. Painter, Coherent optical wavelength conversion via cavity optomechanics, *Nat. Commun.* **3**, 1196 (2012).
- [31] F. Morichetti, A. Canciamilla, C. Ferrari, A. Samarelli, M. Sorel, and A. Melloni, Travelling-wave resonant four-wave mixing breaks the limits of cavity-enhanced all-optical wavelength conversion, *Nat. Commun.* **2**, 296 (2011).
- [32] F. Lecocq, J. B. Clark, R. W. Simmonds, J. Aumentado, and J. D. Teufel, Mechanically Mediated Microwave Frequency Conversion in the Quantum Regime, *Phys. Rev. Lett.* **116**, 043601 (2016).
- [33] M. Xu, X. Han, C. L. Zou, W. Fu, Y. Xu, C. Zhong, L. Jiang, and H. X. Tang, Radiative Cooling of a Superconducting Resonator, *Phys. Rev. Lett.* **124**, 033602 (2020).
- [34] E. Zeuthen, A. Schliesser, A. S. Sørensen, and J. M. Taylor, Figures of merit for quantum transducers, *Quantum Sci. Technol.* **5**, 034009 (2020).
- [35] L. A. Williamson, Y. H. Chen, and J. J. Longdell, Magneto-Optic Modulator with Unit Quantum Efficiency, *Phys. Rev. Lett.* **113**, 203601 (2014).
- [36] L. Ranzani and J. Aumentado, Graph-based analysis of nonreciprocity in coupled-mode systems, *New J. Phys.* **17**, 023024 (2015).
- [37] A. A. Clerk, M. H. Devoret, S. M. Girvin, F. Marquardt, and R. J. Schoelkopf, Introduction to quantum noise, measurement, and amplification, *Rev. Mod. Phys.* **82**, 1155 (2010).
- [38] See Supplemental Material at <http://link.aps.org/supplemental/10.1103/PhysRevResearch.4.L042023> for detailed derivations and discussions, explicit expressions for the parameter regimes, optimal frequencies, and maximal achievable internal efficiencies, and expressions of added noise when the system satisfies the generalized matching condition.
- [39] M. Tsang, Cavity quantum electro-optics. II. Input-output relations between traveling optical and microwave fields, *Phys. Rev. A* **84**, 043845 (2011).
- [40] J. Rahola, Power waves and conjugate matching, *IEEE Trans. Circuits Syst., II, Exp. Briefs* **55**, 92 (2008).
- [41] H.-C. Liu and A. Yariv, Synthesis of high-order bandpass filters based on coupled-resonator optical waveguides (CROWs), *Opt. Express* **19**, 17653 (2011).
- [42] V. Van, Circuit-based method for synthesizing serially coupled microring filters, *J. Lightwave Technol.* **24**, 2912 (2006).
- [43] O. Naaman and J. Aumentado, Synthesis of parametrically coupled networks, *PRX Quantum* **3**, 020201 (2022).
- [44] D. C. Youla, A tutorial exposition of some key network-theoretic ideas underlying classical insertion-loss filter design, *Proc. IEEE* **59**, 760 (1971).
- [45] K. Kurokawa, Power waves and the scattering matrix, *IEEE Trans. Microw. Theory Techn.* **13**, 194 (1965).
- [46] R. Lescanne, S. Deléglise, E. Albertinale, U. Réglade, T. Capelle, E. Ivanov, T. Jacqmin, Z. Leghtas, and E. Flurin, Irreversible Qubit-Photon Coupling for the Detection of Itinerant Microwave Photons, *Phys. Rev. X* **10**, 021038 (2020).
- [47] A. Melloni, F. Morichetti, C. Ferrari, and M. Martinelli, Continuously tunable 1 byte delay in coupled-resonator optical waveguides, *Opt. Lett.* **33**, 2389 (2008).
- [48] F. Xia, L. Sekaric, and Y. Vlasov, Ultracompact optical buffers on a silicon chip, *Nat. Photonics* **1**, 65 (2007).
- [49] C. Zhong, Z. Wang, C. Zou, M. Zhang, X. Han, W. Fu, M. Xu, S. Shankar, M. H. Devoret, H. X. Tang, and L. Jiang, Proposal for Heralded Generation and Detection of Entangled Microwave–Optical-Photon Pairs, *Phys. Rev. Lett.* **124**, 010511 (2020).
- [50] C. Zhong, X. Han, and L. Jiang, Quantum transduction with microwave and optical entanglement, [arXiv:2202.04601](https://arxiv.org/abs/2202.04601).